

Damping transition in an open generalized Aubry-André-Harper model

Peng He,^{1,2} Yu-Guo Liu,^{1,2} Jian-Te Wang,^{1,2} and Shi-Liang Zhu^{3,4,*}

¹*School of Physics, Nanjing University, Nanjing 210093, China*

²*National Laboratory of Solid State Microstructures,*

Collaborative Innovation Center of Advanced Microstructures, Nanjing University, Nanjing 210093, China

³*Guangdong Provincial Key Laboratory of Quantum Engineering and Quantum Materials,*

School of Physics and Telecommunication Engineering,

South China Normal University, Guangzhou 510006, China

⁴*Guangdong-Hong Kong Joint Laboratory of Quantum Matter,*

Frontier Research Institute for Physics, South China Normal University, Guangzhou 510006, China

(Dated: September 28, 2021)

We study the damping dynamics of the single-particle correlation for an open system under aperiodic order, which is dominated by Lindblad master equation. In the absence of the aperiodic order, the Liouvillian superoperator can exhibit the non-Hermitian skin effect, which leads to unidirectional damping dynamics, dubbed as “chiral damping”. Due to the non-Hermitian skin effect, the damping dynamics is boundary sensitive: the long-time damping of such open systems is algebraic under periodic boundary conditions but exponential under open boundary conditions. We reveal a dynamical phase transition with the inclusion of the hopping amplitude modulation. This phase transition is related with emergent non-Bloch anti-PT symmetry breaking, which only occurs under the open boundary condition. When the anti-PT symmetry is broken, the localization property of this system also changes, entering another type with different scaling rules. Furthermore, we propose a possible scheme with ultracold atoms in dissipative momentum lattice to realize and detect the damping dynamics.

I. INTRODUCTION

With advances in manipulating dissipation and quantum coherence in laboratory, the past years have seen a revived interest in the theory of open and non-equilibrium systems [1, 2]. Effective non-Hermitian descriptions have prominently transpired in a plethora of non-conserved systems, such as classical waves with gain and loss [3–8], solids with finite quasiparticle lifetimes [9, 10], and open quantum systems with Markovian reservoir [11, 12] *etc.*. Unique features of non-Hermitian systems have been recognized in various physical contexts, especially in the topological bands [13–16]. For instance, non-Hermitian systems generally possess complex-valued spectra, classified by the homotopy group of general linear group $GL(n, \mathbb{C})$ [15, 17]. The non-Hermitian systems can be gapped in two distinct ways, with a line gap or a point gap. A hallmark of the point-gap topology is failure of the Bloch theorem and the non-Hermitian skin effect (NHSE), namely the anomalous boundary localization for majority of bulk states [14, 18–23].

On the other hand, localization has long time been recognized as important physical implication of scattering, transmission, or interference of waves in dissipative media, since the discovery of Anderson localization [24, 25]. The Anderson localization can occur for lattice with disorder and long-range aperiodic order [24–29]. In recent years, there are growing attentions on the interplay of non-Hermitian physics and disorder effect [30–39]. One

line of work is the characterization and classification of matter phase in terms of disorder [16, 40, 41]. Other topics concern cooperation with coherent control techniques [42]. Disorder, or quasiperiodicity leads to exotic behaviors, including localization-delocalization transition under the PT symmetry breaking [43–45], generalized mobility edges [34] and anomalous particle transport [33], among which the non-Hermitian Aubry-André-Harper (AAH) model provides as a paradigmatic example. However, yet most works only concentrate on non-Hermitian Hamiltonian problems, systems resting on Liouvillians are still rarely studied.

In this work, we consider an open quantum system with aperiodic order, governed by the Lindblad master equation. The aperiodic order is introduced by modulation of lattice hopping amplitude. Following the methods developed in Ref. [46, 47], we study the dynamics of this system in terms of the damping matrix derived from the Liouvillian. The damping matrix is mathematically non-Hermitian. The spectrum and state properties are revealed. We find a phase transition of the state localization with different scaling rules. This phase transition is accompanied by the emergent non-Bloch anti-PT symmetry breaking (reminiscent of the concept of non-Bloch PT symmetry, see Refs. [48, 49]), also signaled by the change of the spectra topology (an imaginary-to-complex transition). The damping dynamics thus exhibits different behaviors. As revealed in Ref. [46], in the absence of the aperiodic order, the system will undergo chiral damping, *i.e.*, the system starts to damp in an unidirectional way. However, with the increase of the aperiodic order, the chiral damping fades away, and the system sees a dynamical phase transition related with non-Bloch anti-PT

*Electronic address: slzhu@nju.edu.cn

symmetry breaking. Furthermore, we propose a possible scheme based on the momentum lattice to realize our model and detect the main physics [50–52].

The rest of this paper is organized as follows. In Sec. II, we briefly review the general framework on how to cast a Liouvillian with linear jump operators to a non-Hermitian damping matrix. In Sec. III, we construct a generalized AAH model, based on a one-dimensional dimerized lattice with modulation of intra-cell hopping amplitude, then discuss the properties of the spectrum and the state. In Sec. IV, we numerically calculate the time evolution of our model, and study the dynamical phase transition. Then we present an experimental proposal for realizing and detecting this model in Sec. V. Finally, a short summary is given in Sec. VI.

II. GENERAL FORMALISM

We start with outlining the Lindblad damping matrix framework for open quantum systems, following Ref. [46]. The dynamics of an open system undergoing Markovian damping is governed by the following Lindblad master equation,

$$\begin{aligned} \frac{d\rho}{dt} &= -i[H, \rho] - \sum_{\mu} (L_{\mu}^{\dagger} L_{\mu} \rho + \rho L_{\mu}^{\dagger} L_{\mu} - 2L_{\mu} \rho L_{\mu}^{\dagger}) \\ &= -i(H_{\text{eff}} \rho - \rho H_{\text{eff}}^{\dagger}) + 2 \sum_i L_{\mu} \rho L_{\mu}^{\dagger}, \end{aligned} \quad (1)$$

where ρ is density matrix, H is the Hamiltonian, L_{μ} 's are the Lindblad jump operators describing coupling to environment. For short-time dynamics before any quantum jump event, when the last term in Eq. (1) is negligible, the system is described by an effective non-Hermitian Hamiltonian $H_{\text{eff}} = H - i \sum_{\mu} L_{\mu}^{\dagger} L_{\mu}$.

We consider noninteracting particles in a tight-binding lattice. The Hamiltonian can be generally written as $H = \sum_{ij} h_{ij} c_i^{\dagger} c_j$, where c_i^{\dagger} (c_i) is the creation (annihilation) operator on lattice site i , and $h_{ij} = h_{ji}^*$ is a time-dependent hopping amplitude ($i \neq j$) or onsite potential ($i = j$). To see the full-time evolution of the density matrix, it is convenient to define the single-particle correlation $\Delta_{ij} = \text{Tr}[c_i^{\dagger} c_j \rho(t)]$. The time evolution then follows $d\Delta_{ij}/dt = \text{Tr}[c_i^{\dagger} c_j d\rho/dt]$. If only the single particle gain and loss, with linear gain dissipator $L_{\mu}^g = \sum_i D_{\mu i}^g c_i^{\dagger}$ and loss dissipator $L_{\mu}^l = \sum_i D_{\mu i}^l c_i$, are concerned, the evolution equation can be recast as,

$$\frac{d\Delta(t)}{dt} = X\Delta(t) + \Delta(t)X^{\dagger} + 2M_g, \quad (2)$$

where $X \equiv ih^T - (M_l^T + M_g)$ is dubbed damping matrix, with $(M_g)_{ij} \equiv \sum_{\mu} D_{\mu i}^{g*} D_{\mu j}^g$ and $(M_l)_{ij} \equiv \sum_{\mu} D_{\mu i}^{l*} D_{\mu j}^l$. Deduction from the single particle correlation of its steady value $\tilde{\Delta}(t) = \Delta(t) - \Delta_s$, homogenizing Eq. (2) gives

$$\tilde{\Delta}(t) = e^{Xt} \tilde{\Delta}(0) e^{X^{\dagger}t}. \quad (3)$$

Here steady state correlation $\Delta_s = \Delta(\infty)$ is determined by $d\Delta_s/dt = 0$, or $X\Delta_s + \Delta_s X^{\dagger} + 2M_g = 0$.

III. MODEL

We consider the following dimerized AAH model [53],

$$H = \sum_{i=1}^N (t_1 + \lambda_i) \hat{c}_{i,A}^{\dagger} \hat{c}_{i,B} + t_2 \hat{c}_{i,B}^{\dagger} \hat{c}_{i+1,A} + \text{h.c.}, \quad (4)$$

where A and B denote two internal degrees of freedom, $\lambda_i = \lambda \cos(2\pi\alpha i + \delta)$ depicts modulation of intra-cell hopping with real parameters λ , α and δ . When $\alpha = p/q$ (with p and q being relatively prime positive integers), the lattice has an enlarged periodicity over q cells, whereas the lattice becomes quasiperiodic with the incommensurate modulation when α is an irrational number. Each unit cell contains a single loss and gain dissipator,

$$L_x^l = \sqrt{\gamma_l/2} (c_{xA} + ic_{xB}), \quad L_x^g = \sqrt{\gamma_g/2} (c_{xA}^{\dagger} + ic_{xB}^{\dagger}). \quad (5)$$

In the commensurate case, the damping matrix is translational invariant with respect to q cells under periodic boundary condition. In the basis

$$\hat{c}_k = (\hat{c}_{1k} \quad e^{-ik/q} \hat{c}_{2k} \quad \dots \quad e^{-i(q-1)k/q} \hat{c}_{qk})^T, \quad (6)$$

the damping matrix in momentum space can be written as

$$\begin{aligned} X(k)_{mn} &= i(\delta_{m,n-1} \bar{t}_m + \delta_{m-1,n} \bar{t}'_n + \delta_{m,1} \delta_{n,2q} t_2 e^{-ik} \\ &\quad + \delta_{m,2q} \delta_{n,1} t_2 e^{ik}) - \frac{\gamma}{2} \mathbb{I}_{2q}, \end{aligned} \quad (7)$$

where $k \in [0, 2\pi]$, $\gamma = \gamma_l + \gamma_g$, \mathbb{I}_{2q} is a $2q \times 2q$ identity matrix, $\bar{t}_{2i-1} = t_1 + \gamma/2 + \lambda_{2i-1}$, $\bar{t}'_{2i-1} = t_1 - \gamma/2 + \lambda_{2i-1}$, and $\bar{t}_{2i}(t'_{2i}) = t_2$. Here to shorten notations we define $\hat{c}_{1k} = (\hat{c}_{1Ak} \quad \hat{c}_{1Bk})$.

We can write X in terms of its right and left eigenvectors,

$$X = \sum_n \lambda_n |u_{Rn}\rangle \langle u_{Ln}|, \quad (8)$$

where $X^{\dagger} |u_{Ln}\rangle = \lambda_n^* |u_{Ln}\rangle$ and $X |u_{Rn}\rangle = \lambda_n |u_{Rn}\rangle$. Then we can also reexpress Eq. (3) as

$$\tilde{\Delta}(t) = \sum_{n,n'} \exp[(\lambda_n + \lambda_{n'}^*)t] |u_{Rn}\rangle \langle u_{Ln} | \tilde{\Delta}(0) |u_{Ln'}\rangle \langle u_{Rn'}|. \quad (9)$$

The long-time behavior of $\tilde{\Delta}$ is dominated by the sector $n = n'$. The Liouvillian spectrum λ_n always holds negative real parts due to the dissipative nature $\text{Re}(\lambda_n) \leq 0$. Therefore the long-time features of the damping dynamics is captured by the Liouvillian gap $\Lambda = \min[2\text{Re}(-\lambda_n)]$. As long as the spectrum is gapped,

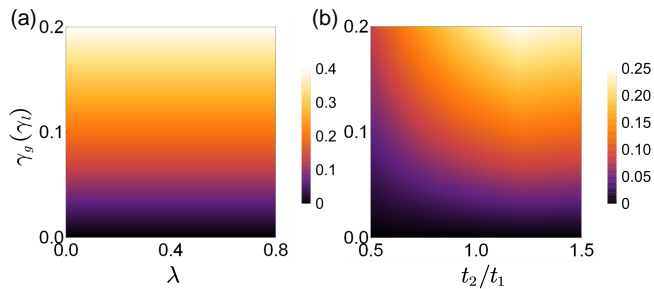


FIG. 1: The phase diagrams of the the Liouvillian gap Λ depends on the dissipation rates $\gamma_g(\gamma_l)$ and (a) the amplitude of the intra-cell hopping modulation λ ; (b) the ratio of the hopping amplitudes t_2/t_1 . The system parameters are $\alpha = 1/4$, $\delta = 0$ and for (a) $t_2/t_1 = 1$; for (b) $\lambda = 1$. Here we consider balanced loss and gain dissipation $\gamma_g = \gamma_l$. And the calculations are carried out with a finite chain with $L = 60$ sites under the OBC.

the system fulfills exponential dissipation. Only a vanishing gap implies algebraic convergence [46]. We numerically calculate the Liouvillian gap under the open boundary condition (OBC). The results are presented in Fig. 1. The Liouvillian gap is dominated by the dissipation rate γ . Other system parameters such as the amplitude of the intra-cell hopping modulation λ and the ratio of the hopping amplitudes t_2/t_1 only play diminishing roles for the long-time exponential damping. However, the modulation of these parameters is essential for the transition of ways to enter the exponential stage, as we will see in the next section.

We compare the complete Liouvillian spectra under the OBC and PBC in Figs. 2 (a-c). The discrepancy between the PBC and OBC spectra in Figs. 2(a) and 2(b) implies the failure of Bloch's theorem and the existence of NHSE, *i.e.*, all the eigenstates of X are exponentially localized at the boundary. Due to the nontrivial boundary effect from the skin modes, the conventional Fourier transformed damping matrix $X(k)$ in Eq. (7) does not reproduce the spectrum structure of an open chain. We use the non-Bloch theory to describe the system under OBC, via complex analytical continuation of the Bloch momentum $k \rightarrow k + i\kappa$ (or $e^{ik} \rightarrow \beta$). The non-Bloch Hamiltonian is given by,

$$X(\beta)_{mn} = i(\delta_{m,n-1}\bar{t}_m + \delta_{m-1,n}t'_n + \delta_{m,1}\delta_{n,2q}t_2\beta^{-1} + \delta_{m,2q}\delta_{n,1}t_2\beta) - \frac{\gamma}{2}\mathbb{I}_{2q}. \quad (10)$$

By solving its characteristic equation $\det(\lambda\mathbb{I}_{2q} - X(\beta)) = 0$, we have a quadratic equation for β with two solutions $\beta_{1,2}$ satisfying

$$\beta_1\beta_2 = \frac{t'_1 t'_3 \cdots t'_{2q-1}}{t_1 t_3 \cdots t_{2q-1}}. \quad (11)$$

In the continuum limit, $|\beta_1| = |\beta_2|$, which gives out $|\beta_{1,2}| = r = \sqrt{|t'_1 t'_3 \cdots t'_{2q-1} / t_1 t_3 \cdots t_{2q-1}|}$. Then the non-Bloch Hamil-

tonian can be obtained by a simple replacement of k with $k + i\kappa = k + i\ln(r)$, or e^{ik} with re^{ik} .

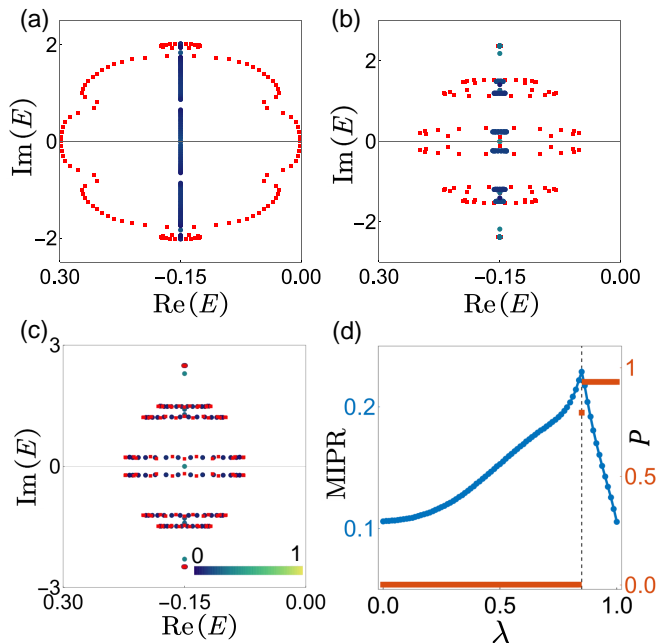


FIG. 2: (a-c) The eigenvalues of the damping matrix on the complex plane under PBC (red squares) and OBC (solid circles), with the color bar indicating the IPR values of the corresponding eigenvectors for (a) $\lambda = 0.2$, (b) $\lambda = 0.85$ and (c) $\lambda = 1.0$ respectively. (d) The MIPR and the real proportion P as the function of modulation amplitude λ for OBC systems with $L = 60$ sites. The dashed line indicates phase transition with the anti-PT symmetry breaking. The other parameters are: $t_1 = t_2 = 1$, $\alpha = 1/4$, $\delta = 0$.

Notably, we find that as λ increases, the OBC system undergoes an emergent non-Bloch anti-PT symmetry breaking, which is reminiscent of the non-Bloch PT symmetry breaking reported in Refs. [48, 49]. Without loss of generality, we consider the lift of the damping matrix X by a constant operation $\tilde{X} = X + \frac{\gamma}{2}\mathbb{I}$, which does not alert the topology of both the spectra and the eigenvectors. \tilde{X} possesses an emergent anti-PT symmetry, provided that $\mathcal{PT}\tilde{X}(\mathcal{PT})^{-1} = -\tilde{X}$ with $\mathcal{PT}c_{i,A(B)}(\mathcal{PT})^{-1} = c_{-i,A(B)}$ and $\mathcal{PT}i(\mathcal{PT})^{-1} = -i$. In the anti-PT symmetric phase, the OBC spectra of \tilde{X} remain purely imaginary [see Fig. 2(a), but with a uniform shift on the real axis], while it becomes complex valued in the anti-PT symmetry broken phase [see Fig. 2(c) and 2(d)]. For the parameter setting chosen here, this phase transition occurs at the critical point $\lambda_c = t_1 - \gamma/2 = 0.85$. To give a more complete description, we numerically calculate the real proportion for \tilde{X} , $P = N_r/N$, where N_r and N denotes the number of eigenvalues with a non-zero real part and all eigenvalues, respectively. The numerical results are shown in Fig. 2(d). The phase transition can be transparently seen at λ_c : for $\lambda < \lambda_c$, the real proportion is almost vanishing $P = 0$, but acquires large values across λ_c .

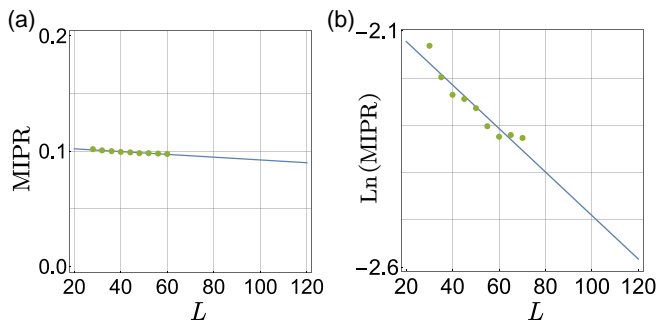


FIG. 3: The MIPR as the function of system length L for (a) $\lambda = 0.2$ and (b) $\lambda = 1$. Other parameters are the same with that of Fig. 2. The dots express the numerical results for distinct system sizes and the solid lines express the interpolation. The scale-free localization in (b) implies immune to skin effect in the anti-PT symmetry broken phase.

Accompanied by the anti-PT symmetry breaking, the localization property dramatically changes because of the competition between the dissipation and hopping modulation. The system enters a critical localization phase with different scaling rules across λ_c , as numerically confirmed in Fig. 3. We calculate the mean inverse participation ratio (MIPR) for a finite open chain,

$$I_m \equiv \frac{1}{L} \sum_{\Lambda} I(\Lambda), \quad I(\Lambda) = \sum_i |u_i(\Lambda)|^4 / [\sum_i |u_i(\Lambda)|^2]^2, \quad (12)$$

where $I(\Lambda)$ is the inverse participation ratio (IPR) for the right eigenvector $|u_R(\Lambda)\rangle$ of X with eigenvalue Λ and $u_i(\Lambda)$ being the i -th entry of $|u_R(\Lambda)\rangle$. As a general rule of thumb, the IPR for an extended state is of the order of $1/L \approx 0$, while a localized state yields finite IPR values. The MIPR behaves non-monotonically due to the interplay of non-Hermiticity and hopping modulation. For a skin localized state $\sim e^{\kappa x}$, the localization length is fixed $\sim 1/|\kappa|$, which is independent of the system size [as numerically confirmed in Fig. 3(a)]. However, in the anti-PT symmetry broken phase, the system exhibits very different scaling behavior, which obeys a logarithmic rule, as shown in Fig. 3(b). The numerical interpolation indicates $\ln(I_m) \approx -0.22 \ln(L) - 1.39$. This means a scale free localization in the symmetry broken phase: the MIPR is proportional to the system size. The transition of the scaling rule implies that localization property is not dominated by the NHSE in the symmetry broken phase. Therefore, the phase transition can be identified both by the spectrum and state properties.

We note that there are nontrivial in-gap modes in the OBC spectra [see Fig. 2(a)-(c)], which is characterized by a winding number (see Appendix A). In this work, we focus on the bulk dynamics, thus these topological modes do not play important roles.

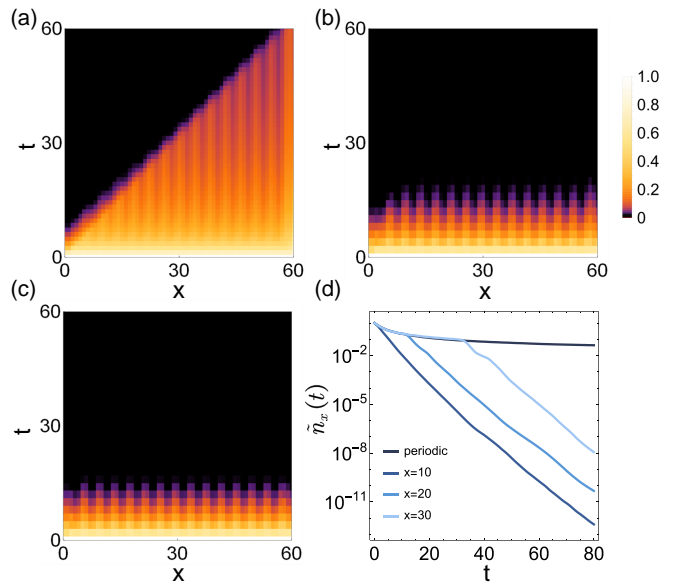


FIG. 4: Time evolution of relative particle number $\tilde{n}_x(t) = n_x(t) - n_x(\infty)$ of an open chain with $L = 60$ sites, for (a) $\lambda = 0.2$, (b) $\lambda = 0.85$, and (c) $\lambda = 1.0$ respectively. (d) shows sectors of (a) at certain lattice sites, compared with the results for a PBC system. Other parameters are the same with that of Fig. 2. The initial state is the completely filled state $\Pi_{x,s} c_{x,s}^\dagger |0\rangle$, *i.e.*, $\Delta(0)$ is a identity matrix.

IV. DAMPING TRANSITION

As a manifestation of the physical implications relevant with the underlying anti-PT symmetry breaking, we perform full-time simulation of the damped system by numerically solving Eq. (3). In the absence of the modulation, or for weak modulation λ , the damping dynamics exhibits chiral features under OBC, dubbed as "chiral damping", as shown in Fig. 4(a). The system always enters exponential damping for a long enough evolution time, due to the finite Liouvillian gap. However, the rapid exponential stage does not immediately start but follows an initial algebraic damping. The initial algebraic damping ends up successively from the left sites to the right sites, forming a sharp "damping wave front", as more clearly seen in Fig. 4(d). This chiral feature fades away as λ increases, and eventually the system only fulfills non-chiral damping across the critical point λ_c .

The chiral damping is attributed to the NHSE, according to Ref. [46]. Intuitively, the asymmetric coupling effectively induces a chiral current, which is associated with the NHSE [54]. To see the role of this current, we decompose the propagator $J_{x'x} = \langle xs | \exp(-iXt) | x's' \rangle$ in terms of the GBZ modes:

$$J_{x'x} \sim \exp(-\gamma t/2) \exp[-\kappa(x - x')], \quad (13)$$

where the term $\exp(-\gamma t/2)$ comes from the background damping [see the last term of Eq. (7)], and the second term is associated with modes acquiring complex momentum $k + i\kappa$. When we can find some existent

site $x' = x - \max(v_k)t (> 0)$ to compensate the background damping, we will have algebraic damping, where $v_k = \text{Im}(\partial\lambda_\beta/\partial k)$ is the group velocity. This indicates a wave front $x = \max(v_k)t$.

The group velocity plays important roles. However, for the modulated cases, λ_β does not have a simple analytic solution. We can also estimate the group velocity by its Lebesgue measure on the imaginary axis: $v_g \sim \Delta W/2$, where the $\Delta W = \sum_l \Delta W_l$ is the Lebesgue measure with ΔW_l being the band width of the spectrum on the imaginary axis. As we have discussed in Sec. III, the spectrum properties dramatically change across the phase transition point. When the NHSE occurs, the system possesses continuous spectrum on the imaginary axis, which gives rise to a finite group velocity and the ballistic current. In contrast, the system possesses discrete point spectrum across λ_c , as shown in Figs. 2(b) and 2(d). The corresponding velocity is vanishing $v_g \sim \Delta W/2 \sim 0$. Intuitively, this leads to dynamical localization thus the damping over the lattice becomes uniform and non-chiral.

We also consider the damping dynamics with incommensurate modulation. The results are presented in Appendix B for comparison.

V. REALIZATION AND DETECTION

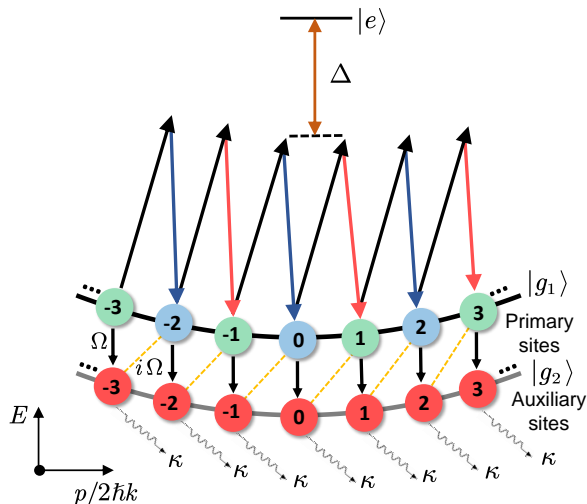


FIG. 5: Schematic illustration of our proposed experimental setup with ultracold atoms in a momentum lattice. The atoms have quadratic free-particle dispersion and are coupled by two-photon Bragg transition with resonant condition $\hbar\omega_n = (2n+1)4E_R$ with E_R being the recoil energy. The Rabi coupling of laser fields $\omega_n^{2(n-1)}$ (illustrated by red arrows) are modulated according to the intracell hopping strength of Hamiltonian (4). Momentum states of atoms in $|g_2\rangle$ are utilized as auxiliary sites to engineer the dissipation. The nearest-neighbor couplings between the primary sites and auxiliary sites, indicated by dashed orange lines, can also be realized with additional Bragg transitions, which are not explicitly illustrated here.

We now propose a scheme to realize the generalized AAH model with ultracold atoms in a momentum lattice [50–52], as illustrated in Fig. 5. We consider ^{87}Rb Bose-Einstein condensate (BEC) in a crossed dipole trap. In the involved $5^2\text{S}_{1/2}$ hyperfine ground state manifold of ^{87}Rb atoms, momentum states in $|g_1\rangle \equiv |1,0\rangle$ encode the lattice sites while another ground state $|g_2\rangle \equiv |2,0\rangle$ with certain decay mode is utilized as auxiliary sites to effectively engineer the desired open dynamics (here the two quantum numbers denote F and m_F for the levels of ^{87}Rb atom).

Two-photon Bragg transitions are utilized to achieve the hopping terms involved in Eq. (4). The simulated two-photon Bragg transitions are driven by pairs of counter-propagating interfering laser fields,

$$\mathbf{E}^+(\mathbf{x}, t) = \mathbf{E}^+ \cos(\mathbf{k}^+ \cdot \mathbf{x} - \omega^+ t + \phi^+), \quad (14)$$

$$\mathbf{E}^-(\mathbf{x}, t) = \sum_n \mathbf{E}_n^- \cos(\mathbf{k}_n^- \cdot \mathbf{x} - \omega_n^- t + \phi_n^-), \quad (15)$$

where $\mathbf{k}^+ = k\hat{x}$ and $\mathbf{k}_j^- = -k\hat{x} \forall j$ with $k = 2\pi/\lambda$. Each pair of the Raman beams $\{\omega_+ \oplus \omega_n^-\}$ couples momentum states $|np_0\rangle$ and $|(n+1)p_0\rangle$, where $p_0 = 2\hbar k$ is the total two-photon recoil momentum transferred from the light fields to the atom. The excited state $|e\rangle$ can be adiabatically eliminated from the Raman transition for a large detuning δ , then the corresponding two-photon Rabi coupling is given by

$$t_n = \tilde{\Omega}_n e^{i\tilde{\phi}_n} = \frac{\Omega_n^* - \Omega^+}{2\Delta} e^{i(\phi^+ - \phi_n^-)}. \quad (16)$$

The hopping rate can be independently modulated to realize the inhomogeneous landscape in Hamiltonian Eq. (4), by tuning the Raman coupling strength Ω_n^- and the phase ϕ_n^- .

With coupling to dissipative auxiliary sites, we can effectively induce the gain and loss process in Eq. (5). Each two nearest-neighbor primary sites are coupled with one auxiliary site (see Fig. 5). The atom loss in the auxiliary sites could be generated by applying a radio frequency pulse to resonantly transfer the atoms in $|g_2\rangle$ to an irrelevant excited state. For a large on-site decay rate $\kappa \gg \Omega$, the decay modes in the auxiliary lattice can be adiabatically eliminated. Thus the effective dynamics is well described by,

$$\dot{\rho} = -i[\tilde{H}, \rho] + \mathcal{D}[L]\rho, \quad (17)$$

$$L = \sum_{\langle i,j \rangle} \sqrt{\tilde{\gamma}}(c_i + ic_j), \quad (18)$$

where $\tilde{\gamma} = \Omega^2/\kappa$ and $\langle i,j \rangle$ runs over all nearest-neighbor sites. We note that Eq. (18) only contains loss dissipators, which are uniformly distributed on the lattice sites thus different from the staggered loss dissipators in Eq.

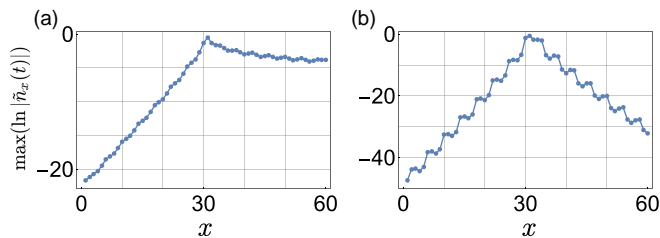


FIG. 6: The maximal value of $\ln|\tilde{n}_x|$ versus lattice site x in terms of the evolution time, for (a) $\lambda = 0.2$ and (b) $\lambda = 1.0$. Other parameters are $t_1/t_2 = 1$, $\tilde{\gamma} = 0.15$, $\alpha = 1/4$, and $\delta = 0$.

(5). However, the proposed experimental setup can still captures the main physics discussed in previous sections.

The observation of the damping dynamics revealed in Sec. IV requires fully filled initial state, which corresponds to a superposition of all target momentum states and is challenging to be prepared in experiments. To escape this problem, we can initialize the system in the zero momentum state, which gives a single occupation at the center site. We numerically calculate the relative particle number $\tilde{n}_x(t)$, and illustrate the maximal value at each site (in the regime of full evolution time) in Fig. 6. As shown in Fig. 6(a), the damping dynamics still exhibits chiral features for weak modulation, due to the preserved NHSE. The signal strength decreases exponentially in the left segment, while it only fulfills a power-law decay in the right segment. This asymmetric decay rate in opposite direction, is dubbed as “information restrain” [55]. As the modulation strength increases, the phenomenon of information restrain fades away, and the signal strength becomes more symmetric in the left and right segments, as shown in Fig. 6(b).

We can also extract the Liouvillian gap from the damping dynamics. We decompose the relative particle number in the biorthogonal eigenbasis,

$$\tilde{n}_x(t) = \sum_{i,j,s} e^{(\lambda_i + \lambda_j^*)t} \langle x, s | u_{Ri} \rangle \langle u_{Li} | u_{Rj} \rangle \langle u_{Lj} | x, s \rangle. \quad (19)$$

For the long-time evolution, the modes with $-\text{Re}(\lambda_i + \lambda_j^*) > \Lambda_g$ can be omitted, thus we can estimate $\tilde{n}_x(t) \approx c e^{-\Lambda_g t}$. Therefore, we can extract the Liouvillian gap from the slope of $\ln(\tilde{n}_x(t)) = \alpha t + \beta$ in the exponential damping stage, by $\alpha \approx -\Lambda_g$. For the parameters in Fig. 6(a), we numerically fit the slope and obtain $\alpha \approx -1.08$, which agrees well with the Liouvillian gap $\Lambda_g \approx 1.00$. In experiments, the local density of state can be detected by the quasimomentum distribution $\rho(k)$ on each spin state from the time-of-flight measurement after abruptly turning off the lattice potential. The atoms in different momentum states evolve to different positions, thus the time-of-flight measurement allows site-resolved detection.

We make some remarks on relevant experimental progress. The Aubry-André model with incommensurate modulation of the on-site potential has been experimentally demonstrated with cold atoms in an optical lattice

[56] and coupled single-mode waveguides [57]. For the experiment with momentum lattice, the topological Anderson insulator has been observed in disordered atomic wires [58]. More recently, a generalized SSH model and a one dimensional quasi-periodic lattice have been realized [59, 60]. The nonreciprocal quantum transport has been successfully observed in a dissipative momentum lattice, which makes it possible to engineer an open quantum system with atoms in a momentum lattice [61].

VI. CONCLUSIONS

In summary, we have investigated the dynamical properties of an open generalized AAH model, in terms of the damping matrix derived from the Liouvillian superoperator. When we tune strength of the modulation of hopping, the damping matrix exhibits a phase transition with anti-PT symmetry breaking. As the phase transition happens, the spectra topology and the scaling rules of eigenvectors dramatically change. The change of the spectral property only occurs when the open boundary condition is imposed, due to the NHSE. We have uncovered the physical consequence by calculating the damping dynamics of the single particle correlation function. The system undergoes a chiral to non-chiral transition as the modulation strength changes. We have also proposed a possible scheme to observe these results based on BEC in a momentum lattice.

Acknowledgments

This work was supported by the Key-Area Research and Development Program of GuangDong Province (Grant No. 2019B030330001), the National Natural Science Foundation of China (Grants No. 12074180 and No. U1801661), and the Key Project of Science and Technology of Guangzhou (No. 2019050001).

Appendix A: Winding number

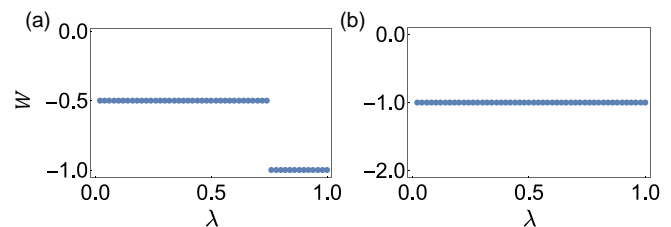


FIG. 7: The winding number versus λ for (a) $\tilde{X}(k)$ and (b) $\tilde{X}(\beta)$ respectively. Other parameters are same with that of Fig. 2.

Without loss of generality, we consider the topological characterization of the compensated damping matrix

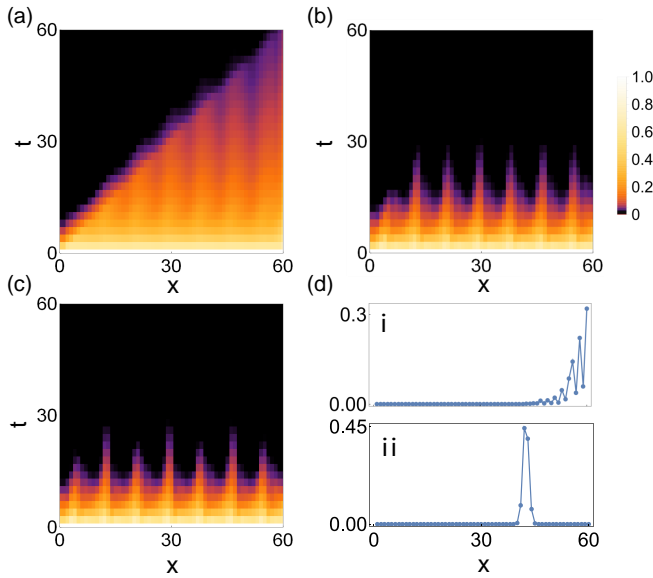


FIG. 8: Time evolution of relative particle number $\tilde{n}_x(t) = n_x(t) - n_x(\infty)$ of an open chain with $L = 60$ sites for (a) $\lambda = 0.2$, (b) $\lambda = 0.85$ and (c) $\lambda = 1.0$, respectively. The lattice is under incommensurate modulation with $\alpha = (\sqrt{5} - 2)/2$. The local density of the L -th eigenvector corresponding to the damping matrix in (a) and (c) is given in (d,i) and (d,ii), respectively.

\tilde{X} . \tilde{X} has a sublattice symmetry, $S^{-1}\tilde{X}S = -\tilde{X}$ with $S = \text{diag}(1, -1, 1, -1, \dots, 1, -1)$, thus we can transform it into an off-diagonal form $\tilde{X} = [0 \ \tilde{X}_1; \tilde{X}_2 \ 0]$, where

$$\tilde{X}_1 = \begin{bmatrix} \bar{t}'_1 & 0 & 0 & \cdots & \bar{t}'_q/\beta \\ \bar{t}'_2 & \bar{t}'_2 & 0 & \cdots & 0 \\ 0 & \bar{t}'_4 & \bar{t}'_5 & \cdots & 0 \\ \vdots & \vdots & \vdots & \ddots & \vdots \\ 0 & 0 & 0 & \cdots & \bar{t}'_{q-1} \end{bmatrix}, \quad \tilde{X}_2 = \begin{bmatrix} \bar{t}'_1 & \bar{t}'_2 & 0 & \cdots & 0 \\ 0 & \bar{t}'_3 & \bar{t}'_4 & \cdots & 0 \\ 0 & 0 & \bar{t}'_5 & \cdots & 0 \\ \vdots & \vdots & \vdots & \ddots & \vdots \\ \bar{t}'_q\beta & 0 & 0 & \cdots & \bar{t}'_{q-1} \end{bmatrix}, \quad (\text{A1})$$

with $\beta \in \mathcal{C}_{\text{GBZ}}$; specifically, when $\beta = k$, it returns to the conventional Brillouin zone. We can define a winding number for each block [16, 35],

$$w_{1,2} = \oint_{\mathcal{C}} \frac{dk}{2\pi i} \partial_k \ln \det \tilde{X}_{1,2}, \quad (\text{A2})$$

then we can define a winding number for the system as $W = (w_1 - w_2)/2$. We calculate the winding number for both $\tilde{X}(k)$ and $\tilde{X}(\beta)$, and the results are presented in Fig. 7. Due to the NHSE, conventional bulk-boundary correspondence breaks down, thus the winding number calculated from \tilde{X}_k can not correctly characterize the topology of an open chain. As shown in Fig. 7(b), the system always has a winding number $W = -1$, which implies that the damping transition is not topological (in terms of the band topology).

Appendix B: Incommensurate case

We study the damping dynamics for the incommensurate case $\alpha = (\sqrt{5} - 2)/2$. As shown in Fig. 8(a)-(c), the damping dynamics shows similar phase transition, compared with Sec. IV. This phase transition is also accompanied by the change of localization properties. The change of localization properties for the incommensurate case can be clearly seen in the local density of the eigenvectors, as shown in Fig. 7(d). The system enters another localization phase across λ_c , where the eigenvectors can be localized at some bulk sites, whereas the skin states always localized on the boundary.

-
- [1] E. J. Bergholtz, J. C. Budich, and F. K. Kunst, Exceptional topology of non-Hermitian systems, *Rev. Mod. Phys.* **93**, 015005 (2021).
- [2] Y. Ashida, Z. Gong, and M. Ueda, Non-Hermitian physics, *Adv. Phys.* **69**, 3 (2020).
- [3] X. Zhu, H. Ramezani, C. Shi, J. Zhu, and X. Zhang, PT-symmetric acoustics, *Phys. Rev. X* **4**, 031042 (2014).
- [4] B. I. Popa and S. A. Cummer, Non-reciprocal and highly nonlinear active acoustic metamaterials, *Nat. Commun.* **5**, 3398 (2014).
- [5] A. Regensburger, C. Bersch, M.-A. Miri, G. Onishchukov, D. N. Christodoulides, and U. Peschel, Parity-time synthetic photonic lattices, *Nature (London)* **488**, 167 (2012).
- [6] L. Feng, Z. J. Wong, R.-M. Ma, Y. Wang, and X. Zhang, Single-mode laser by parity-time symmetry breaking, *Science* **346**, 972 (2014).
- [7] H. Zhou, C. Peng, Y. Yoon, C. W. Hsu, K. A. Nelson, L. Fu, J. D. Joannopoulos, M. Soljacic, and B. Zhen, Observation of bulk Fermi arc and polarization half charge from paired exceptional points, *Science* **359**, 1009 (2018).
- [8] A. Cerjan, S. Huang, M. Wang, K. P. Chen, Y. Chong, and M. C. Rechtsman, Experimental realization of a Weyl exceptional ring, *Nat. Photonics* **13**, 623 (2019).
- [9] V. Kozii and L. Fu, Non-Hermitian topological theory of finite-lifetime quasiparticles: Prediction of bulk Fermi arc due to exceptional point, arXiv:1708.05841 (2017).
- [10] Y. Michishita and R. Peters, Equivalence of the effective non-Hermitian Hamiltonians in the context of open quantum systems and strongly correlated electron systems, *Phys. Rev. Lett.* **124**, 196401 (2020).
- [11] L. Xiao, T. Deng, K. Wang, G. Zhu, Z. Wang, W. Yi, and P. Xue, Observation of non-Hermitian bulk-boundary correspondence in quantum dynamics, *Nat. Phys.* **16**, 761

- (2020).
- [12] L. Xiao, T. Deng, K. Wang, Zhong Wang, Wei Yi, and Peng Xue, Observation of non-Bloch parity-time symmetry and exceptional points, *Phys. Rev. Lett.* **126**, 230402 (2021).
- [13] H. Shen, B. Zhen, and L. Fu, Topological band theory for non-Hermitian Hamiltonians, *Phys. Rev. Lett.* **120**, 146402 (2018).
- [14] S. Yao and Z. Wang, Edge states and topological invariants of non-Hermitian systems, *Phys. Rev. Lett.* **121**, 086803 (2018).
- [15] Z. Gong, Y. Ashida, K. Kawabata, K. Takasan, S. Higashikawa, and M. Ueda, Topological phases of non-Hermitian systems, *Phys. Rev. X* **8**, 031079 (2018).
- [16] K. Kawabata, K. Shiozaki, M. Ueda, and M. Sato, Symmetry and topology in non-Hermitian physics, *Phys. Rev. X* **9**, 041015 (2019).
- [17] K. Kawabata, T. Bessho, and M. Sato, Classification of exceptional points and non-Hermitian topological semimetals, *Phys. Rev. Lett.* **123**, 066405 (2019).
- [18] F. K. Kunst, E. Edvardsson, J. C. Budich, and E. J. Bergholtz, Biorthogonal bulk-boundary correspondence in non-Hermitian Systems, *Phys. Rev. Lett.* **121**, 026808 (2018).
- [19] K. Zhang, Z. Yang, and C. Fang, Correspondence between Winding numbers and skin modes in non-Hermitian systems, *Phys. Rev. Lett.* **125**, 126402 (2020).
- [20] C. H. Lee and R. Thomale, Anatomy of skin modes and topology in non-Hermitian systems, *Phys. Rev. B* **99**, 201103(R) (2019).
- [21] D. S. Borgnia, A. J. Kruchkov, and R.-J. Slager, non-Hermitian Boundary Modes and Topology, *Phys. Rev. Lett.* **124**, 056802 (2020).
- [22] N. Okuma, K. Kawabata, K. Shiozaki, and M. Sato, Topological origin of non-Hermitian skin effects, *Phys. Rev. Lett.* **124**, 086801 (2020).
- [23] K. Yokomizo and S. Murakami, Non-Bloch band theory of non-Hermitian systems, *Phys. Rev. Lett.* **123**, 066404 (2019).
- [24] P. W. Anderson, Absence of Diffusion in Certain Random Lattices, *Phys. Rev.* **109**, 1492 (1958).
- [25] E. Abrahams, P. W. Anderson, D. C. Licciardello, and T. V. Ramakrishnan, Scaling Theory of Localization: Absence of Quantum Diffusion in Two Dimensions, *Phys. Rev. Lett.* **42**, 673 (1979).
- [26] P. G. Harper, Single band motion of conduction electrons in a uniform magnetic field, *Proc. Phys. Soc. London A* **68**, 874 (1955).
- [27] S. Aubry and G. André, Analyticity breaking and Anderson localization in incommensurate lattices, *Ann. Israel Phys. Soc.* **3**, 133 (1980).
- [28] D. R. Hofstadter, Energy levels and wave functions of Bloch electrons in rational and irrational magnetic fields, *Phys. Rev. B* **14**, 2239 (1976).
- [29] S. Y. Jitomirskaya, Metal-insulator transition for the almost Mathieu operator, *Ann. Math.* **150**, 1159 (1999).
- [30] S. Longhi, Topological phase transition in non-Hermitian quasicrystals, *Phys. Rev. Lett.* **122**, 237601 (2019).
- [31] H. Jiang, L.-J. Lang, C. Yang, S.-L. Zhu, and S. Chen, Interplay of non-Hermitian skin effects and Anderson localization in nonreciprocal quasiperiodic lattices, *Phys. Rev. B* **100**, 054301 (2019).
- [32] D.-W. Zhang, Y.-L. Chen, G.-Q. Zhang, L.-J. Lang, Z. Li, and S.-L. Zhu, Skin superfluid, topological Mott insulators, and asymmetric dynamics in an interacting non-Hermitian Aubry-André-Harper model, *Phys. Rev. B* **101**, 235150 (2020).
- [33] S. Longhi, Phase transitions in a non-Hermitian Aubry-André-Harper model, *Phys. Rev. B* **103**, 054203 (2021).
- [34] Q.-B. Zeng and Yong Xu, Winding numbers and generalized mobility edges in non-Hermitian systems, *Phys. Rev. Res.* **2**, 033052 (2020).
- [35] Q.-B. Zeng, Y.-B. Yang, and Y. Xu, Topological phases in non-Hermitian Aubry-André-Harper models, *Phys. Rev. B* **101**, 020201(R) (2020).
- [36] C. Zhang, L. Sheng, and D. Xing, Non-Hermitian disorder-driven topological transition in a dimerized Kitaev superconductor chain, *Phys. Rev. B* **103**, 224207 (2021).
- [37] Y. Liu, Q. Zhou, and S. Chen, Localization transition, spectrum structure and winding numbers for one-dimensional non-Hermitian quasicrystals, arXiv:2009.07605.
- [38] D.-W. Zhang, L.-Z. Tang, L.-J. Lang, H. Yan, and S.-L. Zhu, Non-Hermitian topological Anderson insulators, *Sci. China-Phys. Mech. Astron.* **63**, 267062 (2020).
- [39] K. Kawabata and S. Ryu, Nonunitary scaling theory of non-Hermitian Localization, *Phys. Rev. Lett.* **126**, 166801 (2021).
- [40] A. W. W. Ludwig, Topological phases: classification of topological insulators and superconductors of non-interacting fermions, and beyond, *Phys. Scr.* **2016**, 014001 (2016),
- [41] X. Luo, Z. Xiao, K. Kawabata, T. Ohtsuki, and R. Shindou, Unifying the Anderson transitions in Hermitian and Non-Hermitian systems, arXiv:2105.02514 (2021).
- [42] L. Zhou, Floquet engineering of topological localization transitions in non-Hermitian quasicrystals, arXiv:2106.07149.
- [43] N. Hatano and D. R. Nelson, Localization transitions in non-Hermitian quantum mechanics, *Phys. Rev. Lett.* **77**, 570 (1996).
- [44] N. Hatano and D. R. Nelson, Vortex pinning and non-Hermitian quantum mechanics, *Phys. Rev. B* **58**, 8384 (1998).
- [45] R. Hamazaki, K. Kawabata, and M. Ueda, Non-Hermitian many-body localization, *Phys. Rev. Lett.* **123**, 090603 (2019).
- [46] F. Song, S. Yao, and Z. Wang, Non-Hermitian skin effect and chiral damping in open quantum systems, *Phys. Rev. Lett.* **123**, 170401 (2019).
- [47] C.-H. Liu, K. Zhang, Z. Yang, S. Chen, Helical damping and anomalous critical non-Hermitian skin effect, *Phys. Rev. Research* **2**, 043167 (2020).
- [48] S. Longhi, Non-Bloch PT symmetry breaking in non-Hermitian photonic quantum walks, *Opt. Lett.* **44**, 5804 (2019).
- [49] Stefano Longhi, Probing non-hermitian skin effect and non-bloch phase transitions, *Phys. Rev. Res.* **1**, 023013 (2019).
- [50] B. Gadway, Atom-optics approach to studying transport phenomena, *Phys. Rev. A* **92**, 043606 (2015).
- [51] E. J. Meier, F. A. An, and B. Gadway, Atom-optics simulator of lattice transport phenomena, *Phys. Rev. A* **93**, 051602(R) (2016).
- [52] E. J. Meier, F. A. An, and B. Gadway, Observation of the topological soliton state in the Su-Schrieffer-Heeger model, *Nat. Commun.* **7**, 13986 (2016).

- [53] S. Ganeshan, K. Sun, and S. Das Sarma, Topological Zero-Energy Modes in Gapless Commensurate Aubry-André-Harper Models, *Phys. Rev. Lett.* **110**, 180403 (2013).
- [54] J. Y. Lee, J. Ahn, H. Zhou, and A. Vishwanath, Topological correspondence between Hermitian and Non-Hermitian systems: Anomalous dynamics, *Phys. Rev. Lett.* **123**, 206404 (2019).
- [55] C.-H. Liu and S. Chen, Information restraint in open quantum systems, *arXiv:2012.13583* (2020).
- [56] G. Roati, C. D'Errico, L. Fallani, M. Fattori, C. Fort, M. Zaccanti, G. Modugno, M. Modugno, M. Inguscio, Anderson localization of a non-interacting Bose-Einstein condensate, *Nature (London)* **453**, 895 (2008).
- [57] Y. E. Kraus, Y. Lahini, Z. Ringel, M. Verbin, and O. Zeitun, Topological states and adiabatic pumping in quasicrystals, *Phys. Rev. Lett.* **109**, 106402 (2012).
- [58] E. J. Meier, F. Alex An, A. Dauphin, Observation of the topological anderson insulator in disordered atomic wires. *Science* **362**, 929 (2018).
- [59] D. Xie, W. Gou, T. Xiao, et al., Topological characterizations of an extended Su-Schrieffer-Heeger model. *npj Quantum Inf* **5**, 55 (2019).
- [60] T. Xiao, D. Xie, Z. Dong, T. Chen, W. Yi, B. Yan, Observation of topological phase with critical localization in a quasi-periodic lattice, *Sc. Bull.* **66**(21), 2175 (2021).
- [61] W. Gou, T. Chen, D. Xie, T. Xiao, T. Deng, et. al., Tunable Nonreciprocal Quantum Transport through a Dissipative Aharonov-Bohm Ring in Ultracold Atoms, *Phys. Rev. Lett.* **124**, 070402 (2020).